JACS
JOURNAL OF THE AMERICAN CHEMICAL SOCIETY
Communication
pubs.acs.org/JACS

RCA Strands as Scaffolds To Create Nanoscale Shapes by a Few Staple Strands

Yinzhou Ma,[†] Hongning Zheng,[†] Cuie Wang,[†] Qin Yan,[†] Jie Chao,[‡] Chunhai Fan,[‡] and Shou-Jun Xiao*[,†,§]

[†]State Key Laboratory of Coordination Chemistry, School of Chemistry and Chemical Engineering, Nanjing National Laboratory of Microstructures, Nanjing University, Nanjing 210093, Jiangsu, China

[‡]Laboratory of Physical Biology, Shanghai Institute of Applied Physics, Chinese Academy of Sciences, Shanghai 201800, China

[§]State Key Laboratory of Bioelectronics, Southeast University, Nanjing 210096, Jiangsu, China

Supporting Information

ABSTRACT: Thousands of nucleotide(nt)-long single strand DNAs, generated from rolling-circle-amplification (RCA), were used as scaffolds to create DNA nanoscale wires and plates with a few short staple strands by following the origami design principle with a crossover at 1.5 turns. The core sequence of the circle template, for producing tens and hundreds of tandemly repeated copies of it by RCA, was designed according to Seeman's sequence design principle for nucleic acid structural engineering (Seeman, N. C. *J. Biomol. Struct. Dyn.* **1990**, *8*, 573). The significance for folding the RCA products into nanoscale shapes lies in the design flexibility of both staple and scaffold strand codes, simplicity of a few short staple strands to fold the periodic sequence of RCA products, and lower cost.

The exquisite specificity of Watson–Crick base pairing renders DNA an ideal material for building nanostructures.[1−3] In recent years, the controlled folding of a long single M13mp18 genomic DNA,[4−7] so-called DNA origami, has been developed greatly and utilized in many areas.[6−10] DNA origami, in principle, could avoid the problems of stoichiometry and purification associated with approaches by only using many short oligonucleotides for nanostructural assembly.[4] But it usually takes hundreds of different staple strands to fold a very few available sequence-identified native DNA scaffolds (until now only M13mp18 DNA) into a nanoscale shape.

To simplify the assembly process of DNA origami, e.g., replacing hundreds of different staple strands with a few staple strands, we have endeavored to use RCA products as the scaffold strand to create nanowires, which only needs short staple strands at single-digit level.[11] RCA has been used for sensitivity enhancement in DNA quantitation,[12] mutation detection,[13] and array-based sandwich immunoassay.[14] It is an isothermal, enzymatic amplification process mediated by certain DNA polymerases such as Phi29 DNA polymerase to convert dNTPs into a single strand DNA molecule containing tens and hundreds of tandemly repeated copies of a circularized template strand with about 13−240 nucleotides.[13,15,16] Recently, the use of RCA products for nanoconstruction and biodetection has been reviewed by Li et al.[17] An example was the 1-dimensional periodic assembly of gold nanoparticles.[18] Here, we report the use of the periodic sequence of RCA single strand DNAs (briefly as RCA ssDNAs) to create different kinds of DNA nanowires (DNW) and DNA nanoplates (DNP), demonstrating the feasibility of RCA products for the assembly of many kinds of nanostructures.

As a proof-of-concept, we first designed several DNA nanowires and obtained their AFM images easily. Two examples of DNW-1 and DNW-2 are designed as shown in Figure 1, panels a and b, respectively. DNW-1 illustrates a folding strategy for a linear ssDNA generated from RCA of a 144nt-long circularized template. One 144nt sequence copy was folded by four staple strands (red, 48nt; white, green, and pink, 32nt) into a rectangle of 48 bp × 3 helices (the dotted border in Figure 1a), and the RCA ssDNA continued the same folding configuration to generate the DNW-1 nanowire. Because of the RCA mechanics, one copy is just the complement strand of the template, and all the copies in RCA ssDNAs have the same sequence. So, those four staple strands fold each copy into a rectangle, and these rectangles join together to form a long nanoscale wire with a width of 48 bp.

For DNW-2 in Figure 1b, we designed another folding configuration. The linear ssDNA in DNW-2 was produced by RCA from a 96nt circle template. Each 96nt sequence copy (the dotted border in Figure 1b) was folded into a rectangle of 32 bp × 3 helices with 6 sections of 16nt sequences by four staple strands (red and purple, 32nt; green and yellow, 16nt). The RCA ssDNA continued the same folding configuration to generate the DNW-2 nanowire. The difference between DNW-1 and DNW-2 is that the double helix axis in DNW-1 is perpendicular to the longitudinal direction of the DNW-1 nanowire, while it is parallel in DNW-2.

AFM images of the above two designed structures in air are shown in Figure 1, panels c and d, respectively. The height of DNW-1 is 1 nm, corresponding to a helical height of ∼1.5 nm. According to the design of DNW-1, the theoretical width of the nanowire is 16 nm (4.5 turns). However, due to the well-known AFM "tip broadening" effect, the width of these nanowires was measured as 18 nm. The measurement of

Received: January 4, 2013
Published: February 15, 2013

   dx.doi.org/10.1021/ja400102s | *J. Am. Chem. Soc.* 2013, 135, 2959−2962

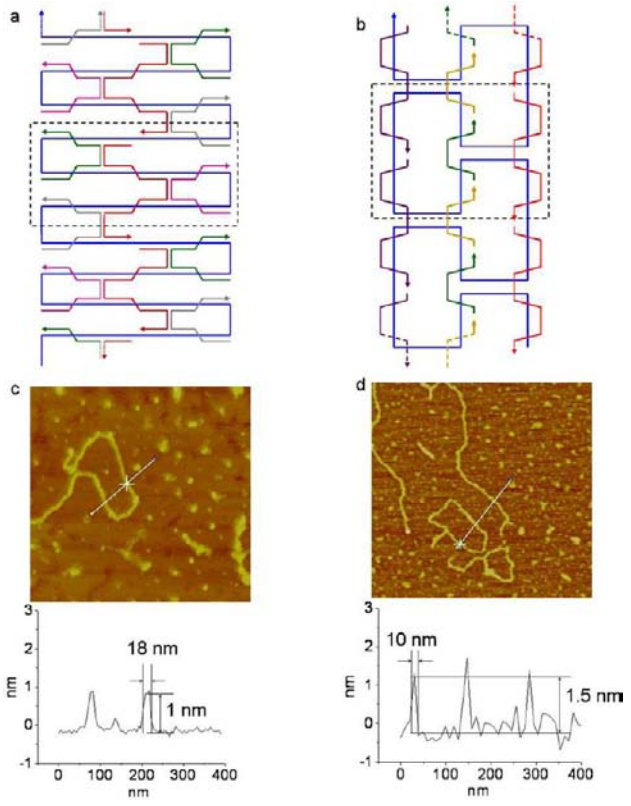

Figure 1. Schematic illustrations and AFM images of DNW-1 from RCA products of a 144nt circle template and DNW-2 from RCA products of a 96nt circle template: (a) the design of a unit of DNW-1 is that a 144nt sequence is folded by four staple strands (red, 48nt; white, green, and pink, 32nt) into a rectangle of 48 bp × 3 helices; (b) the design of a unit of DNW-2 is that a 96nt sequence is folded by four staple strands (red and purple, 32nt; green and yellow, 16nt) into a rectangle of 32 bp × 3 helices; (c) AFM image of DNW-1; (d) AFM image of DNW-2. The basic units of two designs are marked in the dotted borders, respectively.

DNW-2 showed similar results: its height was 1.5 nm, and its width 8 nm which was slightly larger than the theoretical value of 3 helices at 6.0−7.0 nm. Both DNW-1 and DNW-2 nanowires presented respective uniform height and width, meaning the exact folding in experiments as designed. Nanowires can be easily designed, folded, and imaged by AFM with the RCA ssDNAs from different circle templates (more AFM nanowire images with dense coverage and another design were listed in Figures S5 and S6). From our experience, if the template follows Seeman's sequence design principle,[19] the concentration of a template copy unit in RCA ssDNA (considered as the concentration of RCA ssDNA, for details see Section 1.4 of Supporting Information) is in the range of 0.5−1.0 μM and the concentration of staple strands is at around 5−15 times of RCA ssDNA, many alternate designs, by following the origami design principle with a crossover at 1.5 turns (16 bp), will obtain a good yield of nanowires.

Since the RCA ssDNA contains tens and hundreds of tandemly repeating copies of a circularized oligonucleotide, there are several equivalent folding structures for the same set of staple strands, depending on the design. It would be significant if we could fold the RCA ssDNAs with a few staple strands into any 2-dimensional and/or 3-dimensional structures considering lowering the cost of DNA origami and richening the folding strategy with flexibility in designing both staple and scaffold strands. In the next context, we showed an initial result to generate nanowires and further to 2-dimensional nanoplates by folding the RCA ssDNAs from a 96nt circle template with one set of 3 staple strands as designed in Figure 2.

Thermodynamically, the 4 most stable structures with the minimum free-energy path for folding are listed in Figure 2: nanowire of DNW-3 in Figure 2b, nanoplate of DNP-1 in Figure 2e but with 2 possible folding structures of I and II in Figure 2c, and nanoplate of DNP-2 in Figure 2d. Although the folding structures of I and II are slightly different, their morphological appearance should be the similar patterns cartooned as DNP-1. DNP-2 is assembled by joining many individual antiparallel DNW-3 nanowires together with competitive seam-crossing hybridization.[4] To show the configuration of designs clearly, we marked the basic unit of each design with a dotted border. All four designs, following the origami design principle with a crossover at 1.5 turns (16 bp), are folded by the same three staple strands (red, green, and yellow, each with 32nt). A concentration axis for RCA ssDNA is drawn at the bottom, indicating where DNW-3, DNP-1, and DNP-2 will appear, respectively.

Experimentally, we found that the transition between nanowires and two nanoplates was regulated by the concentrations of both RCA ssDNA and staple strands. We first fixed the staple strands at an optimized concentration of 12 μM. As shown in Figure 3, at a low RCA ssDNA concentration of 0.5−1.0 μM, only nanowires of DNW-3 were observed in Figure 3A1−A3, hinting that annealing only occurred in a RCA ssDNA intramolecularly. In the high-resolution AFM image of A3, a uniform height of 1.5 nm and width of 18 nm (slightly larger than the design of 16 nm for 4.5 turns) was measured. However, owing to the repeating sequences, at a higher concentration larger than 1.0 μM, multiple RCA ssDNAs could also be aligned together as in Figure 2c, d and folded to nanoplates. We classified the higher RCA ssDNA concentration into two regions: 1.0−1.5 and 1.5−2.0 μM. At 1.0−1.5 μM, the typical images were shown in Figures 3B1 (9 × 9 μm) and B3 (3 × 3 μm). The low magnification image of B1 showed stiffer and wider nanowires and also reticulate nanoribbon nets, demonstrating a direct transition from nanowires of DNW-3 to nanoribbons of DNP-1. At this transition concentration, both DNW-3 and DNP-1 were grown separately and jointly. The high-resolution image of B3 illustrated the reticulate nanoribbons, where a segment profile in its right gave a uniform height of 2 nm and variable widths from 50 to 100 nm. When the concentration of RCA ssDNA continued to increase to 1.5−2.0 μM, the typical images of reticulate nanoribbons were shown in Figures 3C1 (9 × 9 μm) and C3 (3 × 3 μm), where a segment profile of C3 provided the reticulate nanoribbons with a uniform height of 2 nm and changeable widths of 200−300 nm. These reproducible nanoribbons and joints were suggested to be produced mainly by DNP-1. A notable character was that the width of nanoribbons was changeable. Under the experimental conditions in Figure 3, the ribbon width was roughly proportional to the RCA ssDNA concentration. The nanoribbons in B3 and C3 were different from nanowires of DNW-3 in A3 in 3 points: (1) the nanoribbon width was changeable, depending on the assemblying conditions, while nanowires of DNW-3 always kept a uniform width of 18 nm; (2) the nanoribbon joints were typically higher than other ribbon regions (~1.5 times, see the segment profiles of B3 and C3) due to overlapping of two or more ribbons, joints were everywhere and ribbons between joints were straight and short,

dx.doi.org/10.1021/ja400102s | J. Am. Chem. Soc. 2013, 135, 2959−2962

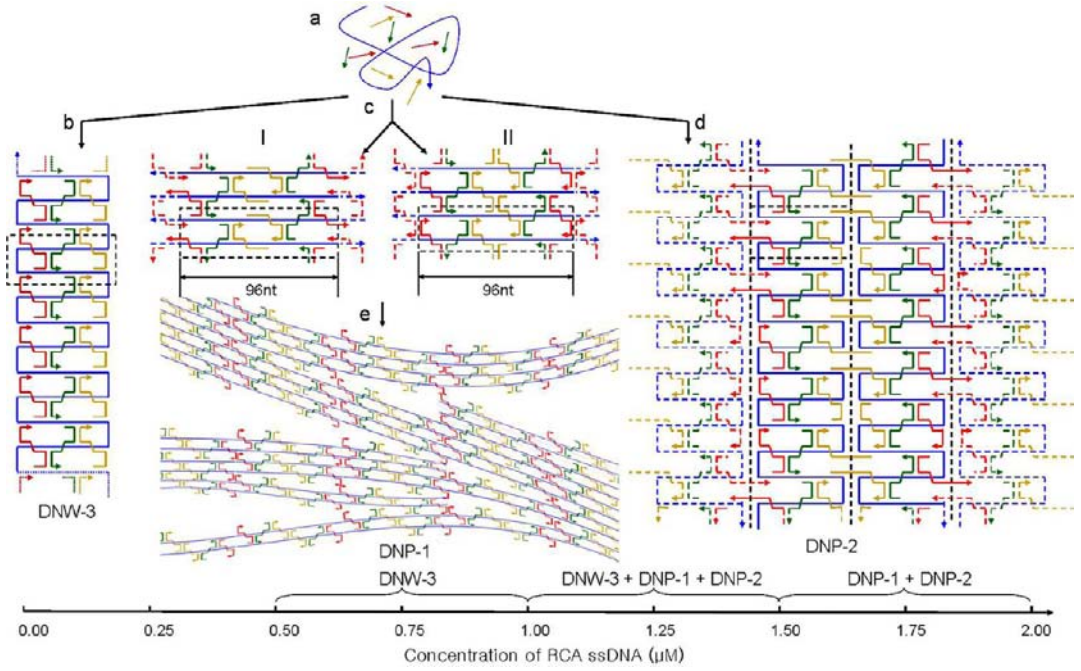

Figure 2. Schematic illustrations of four most possible folding nanostructures from RCA products of a 96nt circle template: (a) mixing staple and RCA ssDNA strands together; (b) folding structure of DNW-3; (c) two basic folding structures of I and II in DNP-1; (d) folding structure of DNP-2 by jointing multiple DNW-3 nanowires together; (e) most possible folding pathway of I and II to generate the morphological appearance of DNP-1. A concentration axis of RCA ssDNA at the bottom demonstrates the concentration-dependent folding structures: at 0.5−1.0 μM, only DNW-3 can be formed; at the transition concentration of 1.0−1.5 μM, both DNW-3 and DNP-1 can be grown separately and jointly; at 1.5−2.0 μM, DNP-1 should dominate the growth; DNP-2 can be grown at 1.0−2.0 μM with a low yield. The molar concentration of staple strands was fixed at 12 μM.

while nanowires in A1∼A3 had much less joints and their curving and bending were clearly seen; (3) the height of nanoribbons was 2 nm, while that of nanowires was 1.5 nm, most possibly due to the easy tip-broadening effect of nanowires.

From our experimental observation, the effect of varying the concentration of scaffold strands (optimized at 0.5−2.0 μM) and the molar ratio of staple strands to scaffold strands (optimized at 5−15) is critical on the assembly of nanostructures. Much lower RCA ssDNA concentrations less than 0.5 μM gave nanowires of DNW-3 in a low density or even nothing when the concentration was too low; while much higher RCA ssDNA concentrations larger than 2.0 μM resulted in much denser and many tangled nanoribbon structures (data not shown). When we fixed the RCA ssDNA concentration at 1.5 μM and changed the concentration of staple strands (Figure S9), nanoribbons were obtained and their widths tended to increase at a molar ratio from 5 to 10, while at a much higher molar ratio over 30, only densely tangled nanowires were observed, due to the much higher hybridization statistic probability of RCA ssDNAs with the surrounded staple strands.

Interestingly, in the high RCA ssDNA concentration region of 1.0−2.0 μM, we observed another kind of nanoplates of DNP-2 in 30% experiments, which were shown in Figure 3B2, C2, D1, and D2. The morphologies of DNP-2 were considerably denser in mass and brighter in height. The high-resolution images of D1 and D2 demonstrated that DNP-2 was isolated from the nanoribbon background of DNP-1, and textured with rigid nanowires possessing clear extending directions. The segment profiles in D1 and D2 illustrated a uniform height of ∼2.5 nm, a width from 200 to 500 nm for general assemblies of 10−25 nanowires of DNW-3, and a length from a few to 10 μm, even longer than the average length of DNW-3 (2−3 μm). Sometimes giant DNA lattices were found, with a size of 6 × 10 μm^2 by joint of parallel DNP-2 nanoplates as shown in Figure S10. The giant lattice could be explained by cross-joining or relay of general DNP-2 assemblies. One specific feature is the striped texture, which should be generated by partial joint among individual DNW-3 nanowires (folding structure see Figure 2d). A perfect seam-crossing joint will result in a homogeneous lattice without seeing the seams in AFM images, which is not the real case in our experiments. The width of the stripe in DNP-2 was measured either with a single nanowire in D1 (18 nm) or 3 nanowires in D2 (60 nm) to calculate a uniform value of ∼18 nm, exactly the width of DNW-3. It was the textured feature that we proposed in the folding structure of DNP-2. However, the detailed mechanism for the high yield of DNP-1 and the low yield of DNP-2 are still unresolved. More AFM images for the 3 designs of DNW-3, DNP-1 and DNP-2 were listed in Figures S7, S8, S10.

In summary, we have designed and created three kinds of nanowires and two kinds of nanoplates with the RCA ssDNAs as scaffolds. Our work demonstrated that many kinds of RCA ssDNAs, where the periodic sequence generated from circularized templates follows Seeman's sequence design principle for nucleic acid structural engineering, could be used for constructing DNA nanoshapes. While a significant loss of control for making exact structures is a flaw and cannot be compared to the conventional DNA origami, RCA still offers a number of distinct advantages in DNA nanotechnology regarding the flexibility of sequence design both for scaffold and staple strands, simplification of tile design with a few staple strands, and lower costs in applications.

dx.doi.org/10.1021/ja400102s | J. Am. Chem. Soc. 2013, 135, 2959−2962

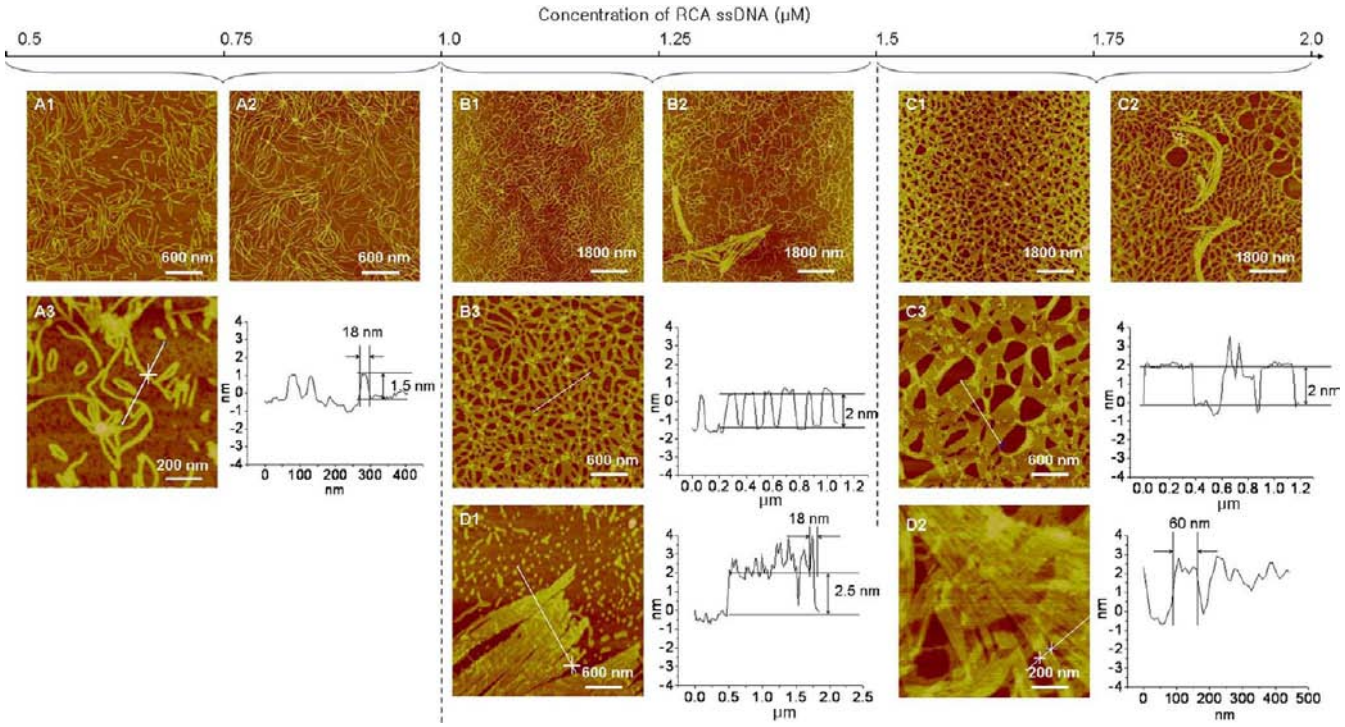

Figure 3. AFM images of DNW-3, DNP-1, and DNP-2 depending on the concentration of RCA ssDNA when the concentration of each staple strand was fixed at 12 μM. When the RCA ssDNA was at 0.5−1.0 μM, only nanowires of DNW-3 were imaged in A1 (3×3 μm^2), A2 (3×3 μm^2), and A3 (1×1 μm^2); when at the transition concentration of 1.0−1.5 μM, both DNW-3 and DNP-1 could be grown separately and jointly, transitions from DNW-3 nanowires to DNP-1 nanoribbons were imaged in B1 (9×9 μm^2) and B3 (3×3 μm^2); when at 1.5−2.0 μM, DNP-1 dominated the growth, nanoribbons mainly from DNP-1 were imaged in C1 (9×9 μm^2) and C3 (3×3 μm^2); nanoplates of DNP-2, shown in low-resolution images of B2 (9×9 μm^2) and C2 (9×9 μm^2) with denser and brighter masses, and in high-resolution images of D1 (3×3 μm^2) and D2 (1×1 μm^2), were observed only in 30% experiments at a RCA ssDNA concentration range between 1.0 and 2.0 μM. Segment profiles are correspondently aligned at the right of each high-resolution image.

■ ASSOCIATED CONTENT

Ⓢ Supporting Information

Experimental procedures, details of each nanostructure sequence code and design, and additional AFM images. This material is available free of charge via the Internet at http://pubs.acs.org.

■ AUTHOR INFORMATION

Corresponding Author

sjxiao@nju.edu.cn

Notes

The authors declare no competing financial interest.

■ ACKNOWLEDGMENTS

We thank the financial support of the National Basic Research Program of China, No. 2013CB922101, NSFC, No. 91027019, No. 21021062, and a funding from the State Key Laboratory of Bioelectronics of Southeast University.

■ REFERENCES

(1) Seeman, N. C. *Nature* **2003**, *421*, 427.
(2) Winfree, E.; Liu, F.; Wenzler, L. A.; Seeman, N. C. *Nature* **1998**, *394*, 539.
(3) He, Y.; Ye, T.; Su, M.; Zhang, C.; Ribbe, A. E.; Jiang, W.; Mao, C. *Nature* **2008**, *452*, 198.
(4) Rothemund, P. W. K. *Nature* **2006**, *440*, 297.
(5) Shih, W. M.; Quispe, J. D.; Joyce, G. F. *Nature* **2004**, *427*, 618.
(6) Han, D.; Pal, S.; Nangreave, J.; Deng, Z.; Liu, Y.; Yan, H. *Science* **2011**, *332*, 342.
(7) Ke, Y.; Sharma, J.; Liu, M.; Jahn, K.; Liu, Y.; Yan, H. *Nano Lett.* **2009**, *9*, 2445.
(8) Voigt, N. V.; Tørring, T.; Rotaru, A.; Jacobsen, M. F.; Ravnsbæk, J. B.; Subramani, R.; Mamdouh, W.; Kjems, J.; Mokhir, A.; Besenbacher, F. *Nat. Nanotechnol.* **2010**, *5*, 200.
(9) Maune, H. T.; Han, S. P.; Barish, R. D.; Bockrath, M.; Goddard, W. A., III; Rothemund, P. W. K.; Winfree, E. *Nat. Nanotechnol.* **2009**, *5*, 61.
(10) Jiang, Q.; Song, C.; Nangreave, J.; Liu, X.; Lin, L.; Qiu, D.; Wang, Z. G.; Zou, G.; Liang, X.; Yan, H. *J. Am. Chem. Soc.* **2012**, *134*, 13396.
(11) Wang, C. E. Ph.D. Thesis, Nanjing University, June 2012.
(12) Nallur, G.; Luo, C.; Fang, L.; Cooley, S.; Dave, V.; Lambert, J.; Kukanskis, K.; Kingsmore, S.; Lasken, R.; Schweitzer, B. *Nucleic Acids Res.* **2001**, *29*, e118.
(13) Lizardi, P. M.; Huang, X.; Zhu, Z.; Bray-Ward, P.; Thomas, D. C.; Ward, D. C. *Nat. Genet.* **1998**, *19*, 225.
(14) Schweitzer, B.; Roberts, S.; Grimwade, B.; Shao, W.; Wang, M.; Fu, Q.; Shu, Q.; Laroche, I.; Zhou, Z.; Tchernev, V. T. *Nat. Biotechnol.* **2002**, *20*, 359.
(15) Fire, A.; Xu, S. Q. *Proc. Natl. Acad. Sci. U.S.A.* **1995**, *92*, 4641.
(16) Liu, D.; Daubendiek, S. L.; Zillman, M. A.; Ryan, K.; Kool, E. T. *J. Am. Chem. Soc.* **1996**, *118*, 1587.
(17) Zhao, W.; Ali, M. M.; Brook, M. A.; Li, Y. *Angew. Chem., Int. Ed.* **2008**, *47*, 6330.
(18) Beyer, S.; Nickels, P.; Simmel, F. C. *Nano Lett.* **2005**, *5*, 719.
(19) Seeman, N. C. *J. Biomol. Struct. Dyn.* **1990**, *8*, 573.